Journal of Materials Chemistry A

ROYAL SOCIETY OF CHEMISTRY

PAPER

Cite this: *J. Mater. Chem. A*, 2020, **8**, 23645

Highly H_2O permeable ionic liquid encapsulated metal–organic framework membranes for energy-efficient air-dehumidification†

Sunghwan Park[a] and Hae-Kwon Jeong *[ab]

Received 7th August 2020
Accepted 21st October 2020

DOI: 10.1039/d0ta07780a

rsc.li/materials-a

Isothermal membrane-based air dehumidification (IMAD) is much more energy-efficient and economical than traditional air-dehumidification technologies. There are, however, no practical IMAD process technologies currently available mainly due to limitations of current membranes. Ionic liquids (ILs) are a promising air-dehumidification membrane material. Current supported IL membranes suffer from poor stability, limiting their performances. Herein, we propose new stable IL membranes, encapsulated IL membranes (EILMs) by encapsulating 1-butyl-3-methylimidazolium bromide ([C_4MIM][Br]) into ultrathin polycrystalline UiO-66-NH_2 metal–organic framework membranes *via* a ship-in-a-bottle method. The stability of IL membranes is significantly enhanced due to the IL entrapped in the pore cages of UiO-66-NH_2. The EILMs show unprecedentedly high H_2O permeance (~2.36 × 10^{-4} mol m^{-2} s^{-1} Pa^{-1}), an order of magnitude greater than that of the most permeable air-dehumidification membranes reported so far. Furthermore, the encapsulated [C_4MIM][Br] drastically increases the H_2O/N_2 separation factor to ~1560, satisfying the minimally required H_2O/N_2 separation performance for commercially viable air-dehumidification.

Introduction

Heating, ventilation, and air-conditioning (HVAC) systems have been critically important for our daily lives. However, more than 90% of the current HVAC systems rely on an energy-intensive vapor compression system, consuming more than 76% of total electricity and ~35% of total energy annually in the U.S.[1] Also, the emission of synthetic refrigerants such as hydrofluorocarbons (HFCs) used in a vapor compression system accelerates global warming.[2] According to the U.S. Department of Energy (DOE), isothermal membrane-based air dehumidification (IMAD) is one of the most promising technologies for energy-efficient and eco-friendly HVAC.[3] In theory, an integrated IMAD and evaporative cooling system can reduce energy consumption by 86.2% as compared to conventional vapor compression.[4]

Membranes of hygroscopic organic liquids such as triethylene glycol (TEG), polyethylene glycol (PEG), and ionic liquids (ILs) have been explored for energy-efficient air-dehumidification due to their superior hydrophilicities.[5–8] As compared to other hygroscopic liquids, ILs are known to be more stable due to their negligible vapor pressures as well as more versatile due to their tailorable properties by the diverse combinations of cations and anions. Current IL membranes (*i.e.*, supported ionic liquid membranes (SILMs)), however, commonly suffer from poor stability and limited performances.[9] In SILMs, ILs are impregnated by capillary force in macro/mesoporous supports, where the ILs can be leached out by pressurization, dissolution, evaporation, *etc.*[10] Accordingly, the IL layers were generally made quite thick (>10 μm) in order to suppress the loss of ILs.[9] Another way to form stable SILMs is to use ILs with high viscosity,[11] which then lower the diffusivity of water vapor. Furthermore, the separation performances of the SILMs impregnated with bulk ILs are likely limited by the slow diffusion of gas molecules from the gas/IL interfaces to the bulk ILs.[12] For example, ILs in contact with CO_2 at the interface were rapidly saturated with CO_2, resulting in a CO_2 saturated dense layer with strong CO_2–IL interactions.[12] Due to the strong interactions, CO_2 diffused slowly from the interface into bulk ILs, lowering the overall efficiency of CO_2 adsorption.[12]

In order to address the above-mentioned challenges of supported IL membranes, there have been several efforts.[9,13,14] Bara *et al.*[15] prepared poly(ionic liquid) membranes by radical polymerization of IL monomers, showing improved mechanical stability. However, the polymerization decreased the separation performance of the membranes due to the restricted mobility of IL fragments.[14] Voss *et al.*[16] developed gelled IL membranes by forming networks of ILs using low molecular-mass organic gelators. The membranes showed enhanced mechanical

[a]*Artie McFerrin Department of Chemical Engineering, Texas A&M University, 3122 TAMU, College Station, TX 77843-3122, USA. E-mail: hjeong7@tamu.edu*

[b]*Department of Materials Science and Engineering, Texas A&M University, 3122 TAMU, College Station, TX 77843-3122, USA*

† Electronic supplementary information (ESI) available. See DOI: 10.1039/d0ta07780a

stability with preserved separation performances. Nevertheless, the gelled IL turned back into liquid with increasing temperature.[13] Friess *et al.*[17] reported polymer/IL mixed-matrix membranes (MMMs) exhibiting promising results. However, these MMMs suffered from limited IL concentration and phase separation due to the stability and the compatibility of ILs.[13] It is, therefore, highly desirable to develop new strategies to fabricate IL membranes that can overcome the trade-off between separation performance and stability.

One of the effective strategies to stabilize ILs is to use the composite of ILs with microporous materials such as metal–organic frameworks (MOFs).[18–20] For example, IL-encapsulated MOFs were found to be effective as catalysts,[21] sorbents,[22] fuel cell membranes,[23] desulfurization,[24] and gas separation membranes.[25,26] There have been several preparation methods reported for IL/MOF composites which can be divided broadly into two categories: (1) ionothermal synthesis and (2) post-impregnation. In ionothermal synthesis, IL/MOF composites were prepared by *in situ* synthesizing MOFs in ILs as a solvent and structure-directing agent.[26] In contrast, post-impregnation methods are more straightforward since ILs were impregnated in preformed MOFs.[18,19] One common post-impregnation method is wet impregnation, where an IL diluted in a solvent is impregnated into MOFs followed by solvent removal.[27] Though this post-impregnation method is simple, leaching of ILs trapped in MOFs is a common issue. Another post-impregnation method is the ship-in-a-bottle method where smaller IL precursors are impregnated and subsequently reacted to form bulkier ILs in MOF cages.[22] It is much less likely for the bulkier ILs encapsulated in the micropore cages of MOFs to leach even under harsh conditions.[22]

Here, we present a new class of supported IL membranes named encapsulated ionic liquid membranes (EILMs). EILMs were prepared by encapsulating ILs in polycrystalline MOF membranes by a ship-in-a-bottle (SIB) strategy. We chose 1-butyl-3-methylimidazolium bromide ([C_4MIM][Br]) and UiO-66-NH_2 MOF membranes as the IL and microporous supports, respectively. The EILMs were thoroughly characterized and the amounts of IL encapsulated were fully determined. The water vapor transport properties of the encapsulated IL were investigated in terms of water vapor sorption and diffusion. Lastly, the H_2O/N_2 separation performances of the EILMs and their stability were tested under various conditions.

Experimental

Materials

For UiO-66-NH_2 synthesis, zirconium(IV) chloride ($ZrCl_4$, >99.5%, Sigma Aldrich), 2-aminoterephthalic acid (H_2BDC-NH_2) ($H_2NC_6H_3$-1,4-$(CO_2H)_2$, 99%, Acros Organics), acetic acid (CH_3CO_2H, >99.7%, Alfa Aesar), and *N*,*N*-dimethylformamide (DMF) ($HCON(CH_3)_2$, >99.8%, Alfa Aesar) were used. For ionic liquid synthesis, 1-methylimidazole (1-MIM) ($C_4H_6N_2$, 99%, Sigma Aldrich) and 1-bromobutane (C_4Br) ($CH_3(CH_2)_3Br$, 99%, Sigma Aldrich) were used. All chemicals were used without further purification.

Preparation of α-alumina supports

α-Alumina supports were prepared by following a recipe reported previously.[28] In a typical preparation, 1.9 g of α-alumina powder (CR6, Baikowski) was homogeneously mixed with 0.2 ml of a polymer binder solution. The binder solution was prepared by dissolving 3 g of polyvinyl alcohol (PVA) (M_w: 22k, Duksan) in a mixture of 5 ml of 1 M HNO_3 and 95 ml of D.I. water. An α-alumina disk was formed by pressing a mold filled with 2.1 g of the alumina/binder mixture uniaxially at 200 bar. Afterwards, the disk was sintered at 1100 °C for 2 h at a ramp rate of 5 °C min^{-1}. The sintered α-alumina disk was polished using sandpaper (grid #1200). The prepared α-alumina disk was 2.2 cm in diameter, 2 mm in thickness, and had 46% porosity with an average pore diameter of ~200 nm.

Synthesis of UiO-66-NH_2 particles

UiO-66-NH_2 particles were synthesized solvothermally based on a recipe reported with a slight modification.[29] A precursor solution was prepared by mixing 0.301 g of $ZrCl_4$, 0.215 g of NH_2-BDC, and 11.63 g of acetic acid in 30 ml of DMF. The prepared solution was placed in a Teflon-lined autoclave. A solvothermal reaction was carried out at 120 °C for 48 h in a convection oven. After completion of the reaction, the autoclave was naturally cooled down to room temperature for 2 h. The powder sample was washed with DMF (30 ml) and collected by centrifugation at 8000 rpm for 15 min. The sample was then further washed with methanol (30 ml) two times. The collected powders were dried under vacuum at 150 °C for 24 h.

Fabrication of UiO-66-NH_2 membranes

The UiO-66-NH_2 membrane was synthesized solvothermally by an *in situ* synthesis method. A metal solution was prepared by mixing 0.471 g of $ZrCl_4$ in 15 ml of DMF followed by solvothermal treatment at 120 °C for 2 h in a Teflon-lined autoclave. For a ligand solution, 0.364 g of H_2BDC-NH_2 was dissolved in 15 ml of DMF, followed by addition of 0.014 g of H_2O and 6.98 g of acetic acid. The ligand solution was poured into a Teflon-lined autoclave containing the metal solution. The solution was thoroughly mixed by magnetic stirring. An α-alumina disk was loaded vertically on a custom-made Teflon holder and then was placed in the solution mixture. Immediately after this, the autoclave was heated at 180 °C for 24 h in a convection oven. The autoclave was cooled down to room temperature for 2 h. The membrane sample was washed with DMF overnight and further washed with methanol for 24 h at room temperature on a lab shaker. It was replenished with fresh methanol every 12 h. The membrane was dried at room temperature for 2 h and then activated at 150 °C under vacuum for 24 h.

Encapsulation of IL in UiO-66-NH_2 particles and membranes

An equimolar mixture of 1-MIM and C_4Br was used to synthesize [C_4MIM][Br]. First, UiO-66-NH_2 powders or membranes were saturated with 1-MIM by stirring for 24 h at room temperature. C_4Br was then added and continuously stirred for 48 h at room temperature. The sample was washed with methanol (30 ml) two times. The sample was dried at 80 °C under vacuum for 24 h.

Fabrication of supported IL membranes (SILMs)

Anodized alumina membranes (Anodisc 25, Whatman) with a pore diameter of 20 nm were used as supports for [C_4MIM][Br] membranes. [C_4MIM][Br] was impregnated into an Anodisc membrane by immersing the membrane in the liquid state IL overnight at room temperature. The prepared SILM was rinsed with methanol and gently blotted by using a Kimwipe. The SILM was supported on a PVDF membrane (Durapore® Membrane filter 0.1 μm, EDM Millipore) to prevent the IL from leaching out.

Characterization

X-ray diffraction (XRD) patterns were taken in a 2θ range of 5–40° with Cu-Kα radiation ($\lambda = 1.5406$ Å) using an X-ray diffractometer (Rigaku Miniflex II). A scanning electron microscope (SEM, JEOL JSM-7500F) was used to investigate the morphology of samples at a working distance of 15 mm and acceleration voltage of 5 keV. Water droplet contact angle measurements were carried out using a fixed volume of water droplets of 5 μl at room temperature. Images were taken using a microscope camera (Motic Moticam 1000) and analyzed by using ImageJ software. Thermogravimetric analysis (TGA, TA instruments Q50) was performed in a temperature range of 25–700 °C with a ramping rate of 10 °C min^{-1} under an air flow of 50 cm^3 min^{-1}. For membrane samples, the weight of the substrates was subtracted after measurements. Solution proton nuclear magnetic resonance (^{1}H NMR) spectra were taken using a Bruker Avance III (400 MHz system). NMR samples were prepared by dissolving in 40 μl D_2SO_4-d2 followed by adding 560 μl DMF-d7. Isothermal N_2 and water vapor physisorption measurements were performed using an ASAP 2020 plus (Micromeritics) at 77.3 K (−195.85 °C) and 293 K (20 °C), respectively. Heat of sorption of water vapor was determined by measuring water sorption at three different temperatures (20 °C, 30 °C, and 40 °C) and an absolute pressure of 1.15 kPa. Kinetic water vapor sorption measurements were conducted with sample loadings of ~0.1 g at 20 °C and at $p/p_o = 0.5$ using ASAP 2020 plus (Micromeritics) using ROA (rate of adsorption) software.

Permeation measurements

H_2O/N_2 separation performances of membranes were tested using a custom-made permeation system shown in Fig. S1.† A humid feed stream was provided by adjusting the ratio of dry N_2 flow rate and water vapor saturated N_2 flow rate. The total flow rates were maintained at 200 cm^3 min^{-1} by using mass flow controllers (MFC, DFC, AALBORG). The feed pressure was adjusted using a back-pressure regulator in the pressure range of 1.5–3.5 bar. The relative humidity was determined by using a dew point meter (HMP7, Vaisala) and was kept at >95%. The permeate side was swept by an argon purge with a flow rate of 100 cm^3 min^{-1}. The permeate side pressure was maintained at ~0.02 bar using a diaphragm pump (N 820.3 FTP, KNF). The compositions of the permeate side were determined using a gas analyzer (QGA, Hiden Analytical). The permeance of component i (P_i) was calculated using the following equation:[30]

$$P_i = \frac{\dot{n}_p \times x_{p,i}}{A\left(p_f \times x_{f,i} - p_p \times x_{p,i}\right)}$$

where, $\dot{n}$ is the total flow rate, x_i is the mole fractions of component i, A is the area of membranes, p is the pressure, and the subscripts p and f are the permeate side and feed side, respectively. The separation factor (α_{ij})was obtained using the equation below;

$$\alpha_{ij} = \frac{x_{p,i}/x_{p,j}}{x_{f,i}/x_{f,j}}$$

Results and discussion

Fabrication and characterization of EILMs

Fig. 1 illustrates the preparation of EILMs by *in situ* synthesizing IL, [C_4MIM][Br], in the cages of a polycrystalline UiO-66-NH_2 membrane *via* a SIB method. UiO-66-NH_2 was selected due to its stability in water vapor and hydrophilicity as well as its processability into polycrystalline membranes.[31] First, a UiO-66-NH_2 membrane was fabricated solvothermally on an α-alumina disk by an *in situ* method (Fig. 1a). It is noted that there have been only two reports on the synthesis of UiO-66-NH_2 membranes,[32,33] both of which required modification of substrates in order to obtain intergrown membranes. In contrast, the membrane was prepared without substrate modification. Instead, we increased both precursor concentrations (both metal and ligand) and the reaction temperature, promoting the intergrowth of UiO-66-NH_2 crystals. The UiO-66-NH_2 membrane was then saturated with 1-MIM followed by addition of C_4Br (Fig. 1b). When these two precursors were reacted, [C_4MIM][Br] IL was formed in the cages of the UiO-66-NH_2 framework. While the precursor molecules can freely diffuse through the 3-dimensionally microporous channels in the framework, the bulkier IL can be trapped in the cages, forming a [C_4MIM][Br]@UiO-66-NH_2 membrane (hereafter, the IL@UiO-66-NH_2 membrane) (Fig. 1c). To form EILMs *via* a SIB method, it is of critical importance to suitably match microporous membranes and ILs. That is to say, IL precursors should penetrate through the ultramicroporous apertures of membranes and yet IL, once formed, should be trapped inside the pore cages.[22,34] UiO-66-NH_2 possesses two different cages, tetrahedral and octahedral ones with the diameters of ~7.5 Å and ~12 Å, respectively, that are interconnected with ~6 Å apertures (Fig. 1).[31] The size of [C_4MIM][Br] was estimated to be ~6–10 Å by the Connolly surface method (Fig. S2†),[35] similar to the diameter obtained from the group contribution method (*i.e.*, ~8 Å).[36] As such, it can be said that UiO-66-NH_2 has suitable sizes of apertures and cages to suitably encapsulate the IL

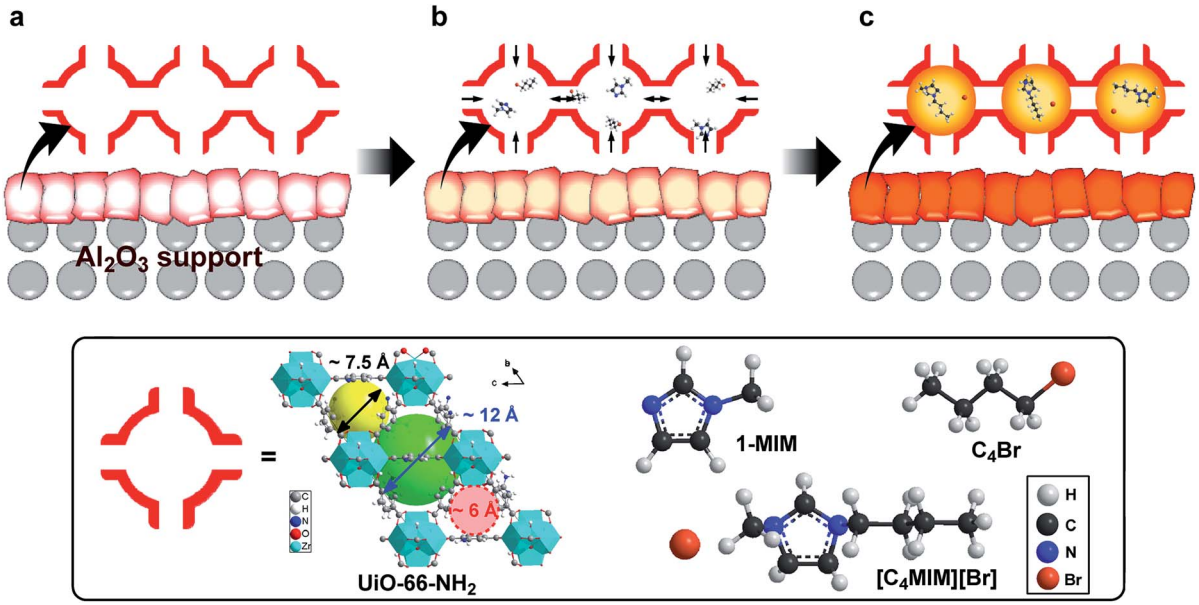

Fig. 1 Scheme of encapsulated ionic liquid membrane (EILM) preparation: (a) preparation of UiO-66-NH_2 membranes, (b) entrapment of IL precursors, and (c) formation of IL@UiO-66-NH_2 membranes upon reaction.

(*i.e.*, 1-MIM & C_4Br < aperture of UiO-66-NH_2 < [C_4MIM][Br] ≈ tetrahedral cage of UiO-66-NH_2 < octahedral cage of UiO-66-NH_2). In addition, considering the fact that the same IL was formed in ZIF-8 and the NaY zeolite by SIB strategies,[34,37] it was inferred that the IL precursors were able to readily pass through the apertures of UiO-66-NH_2.

Fig. 2a presents the XRD patterns of both UiO-66-NH_2 and IL@UiO-66-NH_2 membranes in comparison with a simulated pattern of UiO-66-NH_2 powder. The diffraction pattern of the UiO-66-NH_2 membrane matched well with the simulated one, confirming the formation of a phase-pure UiO-66-NH_2 layer on an alumina support (Fig. 2a). Upon encapsulation of [C_4MIM][Br], the XRD of the IL@UiO-66-NH_2 membrane showed preservation of all peaks, indicating that there was no compromise in the crystal structure of UiO-66-NH_2. Nevertheless, the intensity of the (111) plane was decreased by around a third. As

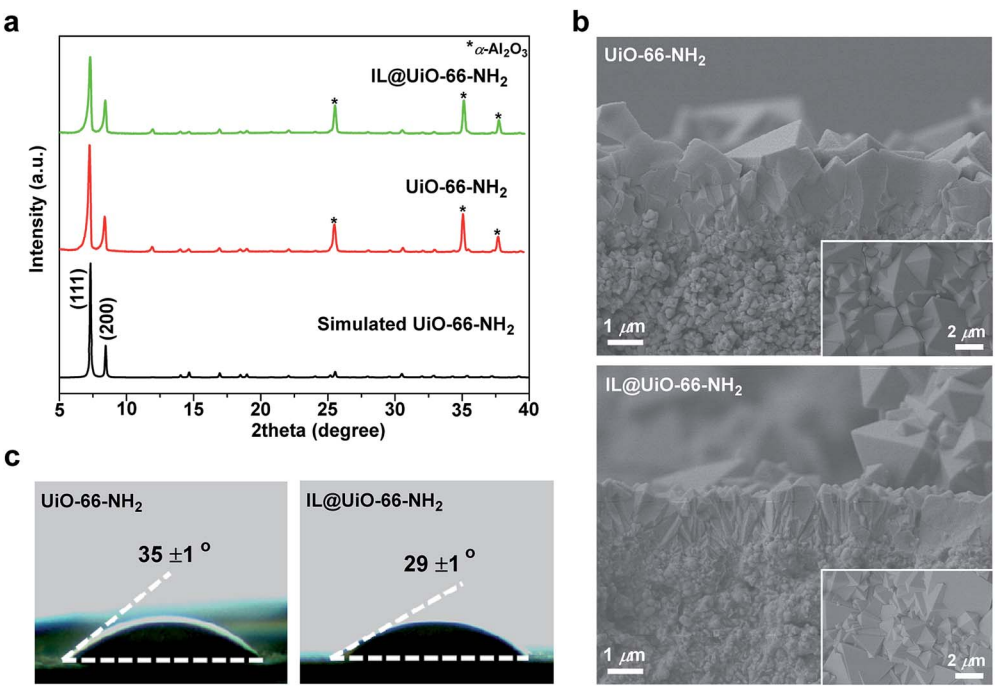

Fig. 2 (a) XRD patterns, (b) SEM images, and (c) water contact angles of UiO-66-NH_2 and IL@UiO-66-NH_2 membranes.

shown in Fig. S3,† the (111) lattice planes are parallel to open triangular apertures surrounding octahedral cages where the encapsulated IL molecules are likely present, thereby leading to the compromise in the diffraction. Fig. 2b presents SEM images showing that UiO-66-NH_2 membranes appeared well-intergrown and defect-free (Fig. 2b top). No crack formation was observed on the membrane upon IL impregnation (Fig. 2b bottom). As expected, the thickness of the membrane remained unchanged at ~2 μm. If confirmed, the IL@UiO-66-NH_2 membranes would be one of the thinnest IL membranes reported.[9,38] Fig. 2c presents water contact angles before and after IL encapsulation. The contact angle decreased upon IL encapsulation, suggesting the presence of hydrophilic [C_4MIM][Br] on the external surface of the EILM.

Quantity analysis of IL encapsulated

Table 1 summarizes the quantity of [C_4MIM][Br] encapsulated in EILMs determined by three different bases (*i.e.*, weight, volume, and mole ratio). According to TGA analysis (Fig. S4†), the residual weight of the UiO-66-NH_2 membrane was 40.7 wt%, which was comparable but slightly lower than the theoretical residual weight of 43.2 wt% possibly due to the absorbed moisture. The theoretical residual weight was determined by assuming that there were no defects in UiO-66-NH_2 crystals and all Zr atoms turned into ZrO_2 upon thermal oxidation. As expected, the IL@UiO-66-NH_2 membrane exhibited greater weight loss upon thermal oxidation than the UiO-66-NH_2 membrane due to the decomposition of the encapsulated [C_4MIM][Br] (Fig. S4†). Based on the difference in the residual weights of the two membranes, the loading percentage of IL (*i.e.*, the mass of IL encapsulated divided by the mass of IL@UiO-66-NH_2) was estimated to be ~19.5 wt%.[39] It should be mentioned that the residual weight of an IL@UiO-66-NH_2 powder sample was consistent with that of an IL@UiO-66-NH_2 membrane sample (see Fig. S5†). Hence, the other two quantitative analyses (*i.e.*, volume and mole ratio) were conducted on powder samples (Fig. S6†).

For volume-based quantification, N_2 adsorption isotherms were taken on UiO-66-NH_2 and IL@UiO-66-NH_2 powder samples. Both showed a type-I isotherm (Fig. S7†), whereas [C_4MIM][Br] showed only negligible N_2 adsorption (*i.e.*, type-III). As can be seen in the isotherms, the pore volume of UiO-66-NH_2 was reduced to ~36.5% upon IL encapsulation (Table 1). This means that ~36.5 vol% of the total pore volume of UiO-66-NH_2 was filled with IL. If some cages are filled with the IL, penetrant precursor molecules are likely to have limited accessibility to other cages. It is, therefore, expected that there exists an optimal IL loading.

Lastly, [C_4MIM][Br] encapsulated was quantified by determining the molar ratio of the UiO-66-NH_2 ligand (*i.e.*, H_2BDC-NH_2) and [C_4MIM][Br] using ^{1}H NMR analysis. As presented in Fig. S8,† the peaks corresponding to [C_4MIM][Br] were found in IL@UiO-66-NH_2, demonstrating the encapsulation of the IL in UiO-66-NH_2. The molar ratio of H_2BDC-NH_2 and [C_4MIM][Br] was estimated to be ~4.1 (Table 1). Since there are 24 ligands per unit cell, about 5.9 [C_4MIM][Br] molecules were encapsulated per unit cell. Based on the molar ratio and the molecular weights of UiO-66-NH_2 and [C_4MIM][Br] (*i.e.*, 6848.1 and 219.1 g mol^{-1}, respectively), the IL loading percentage was back-calculated to be ~15.9 wt%, which is comparable to the TGA result of ~19.5 wt%. There are four tetrahedral and four octahedral cages in the unit cell (Fig. S9†), resulting in the volume of the cages of ~4502.8 Å in a unit cell. Give the molecular volume of [C_4MIM][Br] obtained from the group contribution method (*i.e.*, 285 Å),[36] it was determined that ~37.3% of the cage volume was filled by IL molecules, which was consistent with the N_2 physisorption result of ~36.5%.

Sorption and diffusion of water vapor

Fig. 3 presents water uptake and uptake kinetics of UiO-66-NH_2, [C_4MIM][Br], and IL@UiO-66-NH_2. It should be noted that the measurements were performed on powder samples of UiO-66-NH_2 and IL@UiO-66-NH_2. As can be seen in Fig. 3a, both UiO-66-NH_2 and IL@UiO-66-NH_2 exhibited Langmuir-type isotherms while [C_4MIM][Br] showed a linear isotherm following Henry's law. These observations are consistent with the fact that UiO-66-NH_2 and IL@UiO-66-NH_2 are microporous solids while [C_4MIM][Br] is a dense liquid. IL@UiO-66-NH_2 showed lower adsorption than UiO-66-NH_2 because of its lower micropore volume resulting from IL encapsulation (see Table 1). In the low relative pressure range, UiO-66-NH_2 displayed a concave curve while IL@UiO-66-NH_2 showed a convex curve (see the inset in Fig. 3a). This implies that IL@UiO-66-NH_2 exhibited enhanced interaction with water upon the encapsulation of [C_4MIM][Br],[40] which was corroborated with the fact that the heat of sorption of IL@UiO-66-NH_2 (−54.13 kJ mol^{-1}) was lower than that of UiO-66-NH_2 (−51.76 kJ mol^{-1}) (Table S1†). It is noted that [C_4MIM][Br] showed the highest heat of sorption (−40.01 kJ mol^{-1}), suggesting that water molecules in bulk IL were energetically less favorable than those in the microporous frameworks (Table S1†).[41]

The kinetics of water vapor adsorption of IL@UiO-66-NH_2 was found to be greater than that of UiO-66-NH_2 upon dosing the first aliquot (Fig. 3b). This increase was likely due to the presence of encapsulated [C_4MIM][Br]. It is noteworthy to mention that [C_4MIM][Br] showed the fastest water vapor

Table 1 Quantification of encapsulated [C_4MIM][Br] in UiO-66-NH_2

Sample	Residual weight[a] (wt%)	Pore volume[b] (cm^3 g^{-1})	Molar ratio of H_2BDC-NH_2/[C_4MIM][Br][b]
UiO-66-NH_2	40.7 ± 1.3	0.351 ± 0.008	n/a
IL@UiO-66-NH_2	35.6 ± 0.6	0.223 ± 0.005	4.1 ± 1.6

[a] Membrane samples. [b] Powder samples.

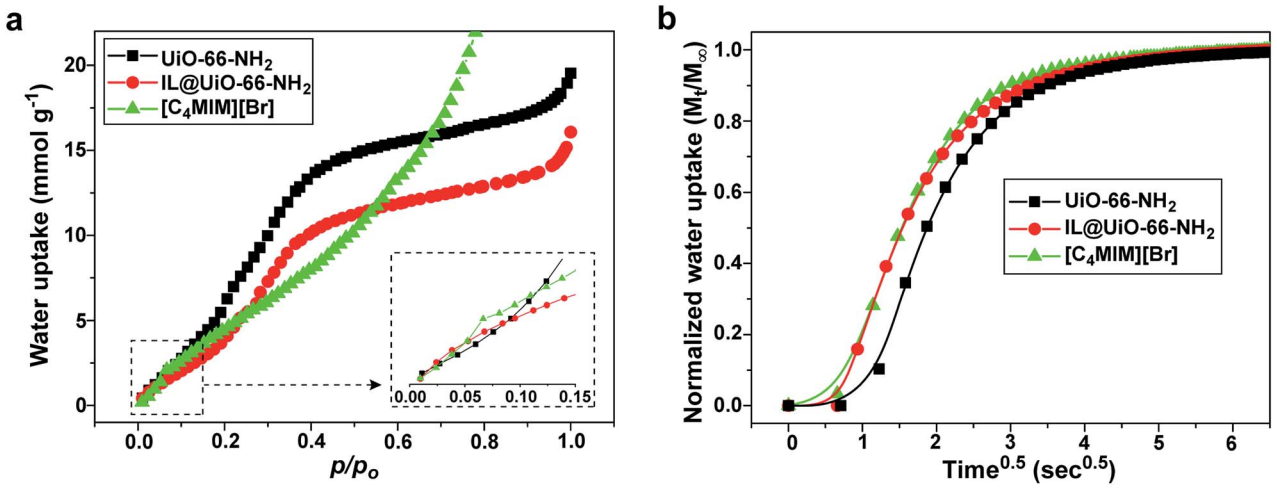

Fig. 3 (a) Water vapor absorption isotherms at 20 °C and (b) uptake kinetics of water vapor at 20 °C and $p/p_o = 0.5$ with the first aliquot dosing. The inset in (a) shows magnified isotherms in the range of $p/p_o = 0.00–0.15$. For clarity, the water update isotherm of the IL was cut at $p/p_o \sim 0.78$ due to its exceptionally high uptake as compared to the other samples.

adsorption among the samples (see Fig. 3b). Pertaining to the non-steady state initial sorption rate (*i.e.*, linear region up to 0.5 of the equilibrium values), it was possible to calculate the effective diffusion coefficients (D_{eff}) graphically using the sorption-time curves (Table S2†). The detailed calculation is presented in the ESI.† The D_{eff} values increased in the following order: 4.91×10^{-11} cm^2 s^{-1} for UiO-66-NH$_2$ < 6.01×10^{-11} cm^2 s^{-1} for IL@UiO-66-NH$_2$ < 2.22×10^{-7} cm^2 s^{-1} for [C$_4$MIM][Br]. The D_{eff} of IL@UiO-66-NH$_2$ was ~22% greater than that of UiO-66-NH$_2$, whereas that of [C$_4$MIM][Br] was four orders of magnitude higher than that of the other two.[42] For overall dosing, however, the absorption rate of bulk [C$_4$MIM][Br] was significantly lower than those of UiO-66-NH$_2$ and IL@UiO-66-NH$_2$ (Fig. S10†). For the first aliquot dosing, the sorption of water in bulk [C$_4$MIM][Br] occurs mainly at the air/IL interface. However, once the interfacial region is saturated, water molecules may need to penetrate deeper into the bulk IL, consequently decreasing the overall adsorption kinetics. For the overall dosing, the water diffusion of IL@UiO-66-NH$_2$ was still faster than that of UiO-66-NH$_2$ (Fig. S10†). This reveals that encapsulated [C$_4$MIM][Br] was considerably more efficient than bulk [C$_4$MIM][Br] due to the increased contact surface area of IL with water molecules. Furthermore, the viscosity effect of [C$_4$MIM][Br], which plays a significant role in a bulk phase, might be negligible since [C$_4$MIM][Br] is dispersed in the cages at the molecular level, therefore IL@UiO-66-NH$_2$ shows enhanced diffusion of water vapor as compared to [C$_4$MIM][Br].

H$_2$O/N$_2$ separation performances of EILMs and their stability

The H$_2$O/N$_2$ separation performances of EILMs were evaluated by comparing with the previously reported air-dehumidification membranes (Fig. 4a and Table S3†).[5–7,30,43–55] It turned out that there were a couple of studies reported on the minimally required H$_2$O/N$_2$ separation performances of membranes for energy effective air-dehumidification.[56,57] According to those studies,[56,57] the water permeance should be at least 5×10^{-6} mol m^{-2} s^{-1} Pa^{-1} (*i.e.*, 14 900 GPU) and the required H$_2$O/N$_2$ selectivity ought to be 1000 and greater (Fig. 4a). There were, however, only a few graphene-oxide (GO) membranes that satisfied the criteria so far.[54,55] Surprisingly, the IL@UiO-66-NH$_2$ membranes met the criteria under mixed gas conditions while both UiO-66-NH$_2$ and [C$_4$MIM][Br] membranes failed to meet the criteria (Fig. 4a). In particular, the IL@UiO-66-NH$_2$ membranes showed the average H$_2$O permeance of 2.36×10^{-4} mol m^{-2} s^{-1} Pa^{-1} which is, to the best of our knowledge, the highest H$_2$O permeance ever reported (Fig. 4a). This exceptionally high H$_2$O permeance can be attributed to the ultrathin nature of the membrane as well as to the enhanced efficiency of encapsulated [C$_4$MIM][Br]. Meanwhile, the H$_2$O permeance of the [C$_4$MIM][Br] membranes (*i.e.*, supported IL membrane) was as low as other supported liquid membranes reported owing to its lower efficiency as well as its greater thickness.[5–7] As compared to the UiO-66-NH$_2$ membranes, the IL@UiO-66-NH$_2$ membranes exhibited a much enhanced H$_2$O/N$_2$ separation factor (~1564 *vs.* ~312) due to the presence of the highly water selective [C$_4$MIM][Br] (note that the H$_2$O/N$_2$ separation factor of the IL was ~4206).

Stability of the membrane is important for practical applications. As shown in Fig. 4b, the H$_2$O permeances of both UiO-66-NH$_2$ and IL@UiO-66-NH$_2$ membranes were well-maintained during 7 days of operation. However, the [C$_4$MIM][Br] liquid membrane showed unstable H$_2$O permeability with time (Fig. 4b). After a couple of days, the H$_2$O permeability of the [C$_4$MIM][Br] membrane decreased and then suddenly increased sharply. Typically, ILs were immobilized in supports by a high capillary force and a high viscosity.[58] As such, the stability of supported IL membranes is greatly affected by the properties of both ILs and supports. The unstable performance of the [C$_4$MIM][Br] membrane is likely due to its relatively low viscosity and high solubility with the water vapor of the feed stream.[59] As the water content in [C$_4$MIM][Br] increased upon extended

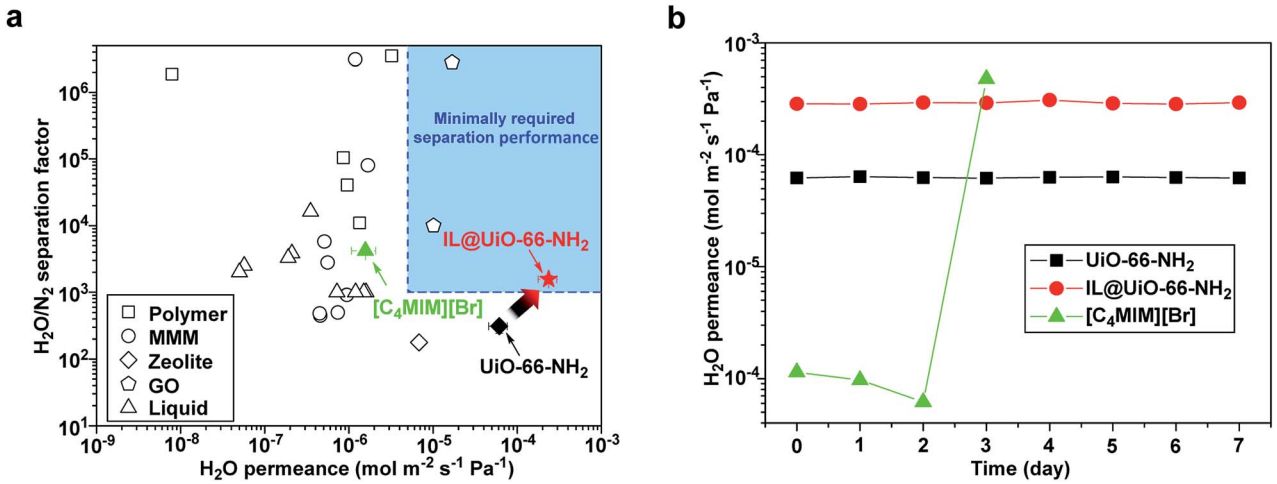

Fig. 4 (a) H_2O/N_2 separation performance of the EILMs compared with those reported in the literature[5–7,30,43–55] and (b) time-dependent H_2O permeances at 20 °C and 1.5 bar of feed pressure.

operation, viscosity of [C4MIM][Br] was likely further reduced,[60] thereby leading to leaching of $[C_4MIM][Br]$ from the support.[10] On the other hand, $[C_4MIM][Br]$ was trapped in the cages of the UiO-66-NH_2 membranes, making it difficult for the IL to leach out even under high humidity conditions. As a consequence, the EILM showed stable separation performance over 7 days of operation. The stability of the IL membranes under various conditions was also tested. At the higher feed pressure and temperature, the IL@UiO-66-NH_2 showed significantly improved separation performances compared to $[C_4MIM][Br]$ membranes (Fig. S11 and S12†).

Conclusions

In conclusion, we successfully formed the encapsulated ionic liquid membranes (EILMs) by encapsulating $[C_4MIM][Br]$ in polycrystalline UiO-66-NH_2 MOF membranes *via* a ship-in-a-bottle method. The resulting EILMs (*i.e.*, $[C_4MIM][Br]$@UiO-66-NH_2 membranes) were ~2 μm thick, one of the thinnest IL membranes reported. It was found that the loading percentage of the encapsulated $[C_4MIM][Br]$ was ~19.5 wt%, occupying ~36.5 vol% of the total cage volume of UiO-66-NH_2. Although the IL-encapsulated UiO-66-NH_2 membranes showed slightly lower water vapor uptake due to their reduced free pore volume, they showed greater affinity to water vapor than the as-prepared UiO-66-NH_2 owing to the presence of the hydrophilic IL. The IL@UiO-66-NH_2 membranes showed increased water vapor uptake kinetics, thereby enhancing H_2O permeance. The EILMs exhibited the highest H_2O permeance among air-dehumidification membranes reported due to the (1) enhanced IL efficiency upon encapsulation and (2) ultrathin nature of the microporous framework membranes. Furthermore, encapsulation of the IL substantially increased the H_2O/N_2 separation factor of the membranes from ~312 to ~1564. Finally, the EILMs displayed noticeably enhanced stability for H_2O/N_2 separation as compared with the $[C_4MIM][Br]$ SILMs under various operation conditions. The current EILMs are expected to be a major step forward in the development of practical air-dehumidification membranes for energy-efficient HVAC systems.

Conflicts of interest

There are no conflicts to declare.

Acknowledgements

H.-K. J. acknowledges the financial support from the National Science Foundation (CBET-1510530 and CBET-1929596). This publication was made possible in part by NPRP12S-0128-190016 from the Qatar National Research Fund (a member of the Qatar Foundation). The findings achieved herein are solely the responsibility of the authors. The National Science Foundation supported the FE-SEM acquisition under grant DBI-0116835, the VP for Research Office, and the Texas A&M Engineering Experimental Station. The authors would like to thank Dr Fernando Soto in Chemical Engineering at Texas A&M University for his help in obtaining the Connolly surfaces.

References

1 P. D. Holtberg, J. J. Conti, J. R. Diefenderfer, S. A. Napolitano, M. Schaal, J. T. Turnure and L. D. Westfall, *Annual Energy Outlook 2014*, U.S. Energy Information Administration (EIA), Washington, DC, 2014.

2 M. F. Lunt, M. Rigby, A. L. Ganesan, A. J. Manning, R. G. Prinn, S. O'Doherty, J. Muhle, C. M. Harth, P. K. Salameh, T. Arnold, R. F. Weiss, T. Saito, Y. Yokouchi, P. B. Krummel, L. P. Steele, P. J. Fraser, S. L. Li, S. Park, S. Reimann, M. K. Vollmer, C. Lunder, O. Hermansen, N. Schmidbauer, M. Maione, J. Arduini, D. Young and P. G. Simmonds, *Proc. Natl. Acad. Sci. U. S. A.*, 2015, **112**, 5927–5931.

3 R. Z. William Goetzler and J. Young, *Caitlin Johnson, Energy Savings Potential and RD&D Opportunities for Non-vapor-*

compression HVAC Technologies, U.S. Department of Energy, 2014.
4 H. T. El-Dessouky, H. M. Ettouney and W. Bouhamra, *Chem. Eng. Res. Des.*, 2000, **78**, 999–1009.
5 A. Ito, *J. Membr. Sci.*, 2000, **175**, 35–42.
6 P. Scovazzo, *J. Membr. Sci.*, 2010, **355**, 7–17.
7 A. Kudasheva, T. Kamiya, Y. Hirota and A. Ito, *J. Membr. Sci.*, 2016, **499**, 379–385.
8 M. Qu, O. Abdelaziz, Z. M. Gao and H. X. Yin, *Renewable Sustainable Energy Rev.*, 2018, **82**, 4060–4069.
9 L. J. Lozano, C. Godínez, A. P. de los Ríos, F. J. Hernández-Fernández, S. Sánchez-Segado and F. J. Alguacil, *J. Membr. Sci.*, 2011, **376**, 1–14.
10 W. Zhao, G. H. He, F. Nie, L. L. Zhang, H. C. Feng and H. J. Liu, *J. Membr. Sci.*, 2012, **411**, 73–80.
11 M. A. Malik, M. A. Hashim and F. Nabi, *Chem. Eng. J.*, 2011, **171**, 242–254.
12 M. E. Perez-Blanco and E. J. Maginn, *J. Phys. Chem. B*, 2010, **114**, 11827–11837.
13 B. Sasikumar, G. Arthanareeswaran and A. F. Ismail, *J. Mol. Liq.*, 2018, **266**, 330–341.
14 H. Gao, L. Bai, J. Han, B. Yang, S. Zhang and X. Zhang, *Chem. Commun.*, 2018, **54**, 12671–12685.
15 J. E. Bara, S. Lessmann, C. J. Gabriel, E. S. Hatakeyama, R. D. Noble and D. L. Gin, *Ind. Eng. Chem. Res.*, 2007, **46**, 5397–5404.
16 B. A. Voss, J. E. Bara, D. L. Gin and R. D. Noble, *Chem. Mater.*, 2009, **21**, 3027–3029.
17 K. Friess, J. C. Jansen, F. Bazzarelli, P. Izák, V. Jarmarová, M. Kačírková, J. Schauer, G. Clarizia and P. Bernardo, *J. Membr. Sci.*, 2012, **415–416**, 801–809.
18 S. Zhang, J. Zhang, Y. Zhang and Y. Deng, *Chem. Rev.*, 2017, **117**, 6755–6833.
19 F. P. Kinik, A. Uzun and S. Keskin, *ChemSusChem*, 2017, **10**, 2842–2863.
20 K. Fujie and H. Kitagawa, *Coord. Chem. Rev.*, 2016, **307**, 382–390.
21 Q.-x. Luo, M. Ji, M.-h. Lu, C. Hao, J.-s. Qiu and Y.-q. Li, *J. Mater. Chem. A*, 2013, **1**, 6530–6534.
22 N. A. Khan, Z. Hasan and S. H. Jhung, *Chem. Commun.*, 2016, **52**, 2561–2564.
23 Z. Li, W. Wang, Y. Chen, C. Xiong, G. He, Y. Cao, H. Wu, M. D. Guiver and Z. Jiang, *J. Mater. Chem. A*, 2016, **4**, 2340–2348.
24 N. A. Khan, Z. Hasan and S. H. Jhung, *Chem.–Eur. J.*, 2014, **20**, 376–380.
25 L. Hao, P. Li, T. Yang and T.-S. Chung, *J. Membr. Sci.*, 2013, **436**, 221–231.
26 Y. J. Ban, Z. J. Li, Y. S. Li, Y. Peng, H. Jin, W. M. Jiao, A. Guo, P. Wang, Q. Y. Yang, C. L. Zhong and W. S. Yang, *Angew. Chem., Int. Ed.*, 2015, **54**, 15483–15487.
27 J. Ma, Y. Ying, X. Guo, H. Huang, D. Liu and C. Zhong, *J. Mater. Chem. A*, 2016, **4**, 7281–7288.
28 H. T. Kwon and H.-K. Jeong, *Chem. Commun.*, 2013, **49**, 3854–3856.
29 F. Wu, L. Lin, H. Liu, H. Wang, J. Qiu and X. Zhang, *J. Membr. Sci.*, 2017, **544**, 342–350.
30 R. Xing, Y. X. Rao, W. TeGrotenhuis, N. Canfield, F. Zheng, D. W. Winiarski and W. Liu, *Chem. Eng. Sci.*, 2013, **104**, 596–609.
31 P. M. Schoenecker, C. G. Carson, H. Jasuja, C. J. J. Flemming and K. S. Walton, *Ind. Eng. Chem. Res.*, 2012, **51**, 6513–6519.
32 L. Wan, C. Zhou, K. Xu, B. Feng and A. Huang, *Microporous Mesoporous Mater.*, 2017, **252**, 207–213.
33 F. Wu, Y. Cao, H. Liu and X. Zhang, *J. Membr. Sci.*, 2018, **556**, 54–65.
34 Y. Yu, J. Mai, L. Wang, X. Li, Z. Jiang and F. Wang, *Sci. Rep.*, 2014, **4**, 5997–6004.
35 M. L. Connolly, *J. Appl. Crystallogr.*, 1983, **16**, 548–558.
36 R. L. Gardas and J. A. P. Coutinho, *Fluid Phase Equilib.*, 2008, **266**, 195–201.
37 I. Ahmed, T. Panja, N. A. Khan, M. Sarker, J.-S. Yu and S. H. Jhung, *ACS Appl. Mater. Interfaces*, 2017, **9**, 10276–10285.
38 P. T. Nguyen, B. A. Voss, E. F. Wiesenauer, D. L. Gin and R. D. Nobe, *Ind. Eng. Chem. Res.*, 2013, **52**, 8812–8821.
39 S. H. Shen, Y. S. Wu, Y. C. Liu and D. C. Wu, *Int. J. Nanomed.*, 2017, **12**, 4085–4109.
40 S. Brunauer, L. S. Deming, W. E. Deming and E. Teller, *J. Am. Chem. Soc.*, 1940, **62**, 1723–1732.
41 A. Deyko and R. G. Jones, *Faraday Discuss.*, 2012, **154**, 265–288.
42 M. A. Rocha and M. B. Shiflett, *Ind. Eng. Chem. Res.*, 2019, **58**, 1743–1753.
43 S. J. Metz, W. J. C. van de Ven, J. Potreck, M. H. V. Mulder and M. Wessling, *J. Membr. Sci.*, 2005, **251**, 29–41.
44 S. M. Allen, M. Fujii, V. Stannett, H. B. Hopfenberg and J. L. Williams, *J. Membr. Sci.*, 1977, **2**, 153–163.
45 H. Sijbesma, K. Nymeijer, R. van Marwijk, R. Heijboer, J. Potreck and M. Wessling, *J. Membr. Sci.*, 2008, **313**, 263–276.
46 T. Puspasari, F. H. Akhtar, W. Ogieglo, O. Alharbi and K. V. Peinemann, *J. Mater. Chem. A*, 2018, **6**, 9271–9279.
47 T. D. Bui, F. Chen, A. Nida, K. J. Chua and K. C. Ng, *Sep. Purif. Technol.*, 2015, **144**, 114–122.
48 D. T. Bui, A. Nida, K. C. Ng and K. J. Chua, *J. Membr. Sci.*, 2016, **498**, 254–262.
49 F. H. Akhtar, M. Kumar and K.-V. Peinemann, *J. Membr. Sci.*, 2017, **525**, 187–194.
50 M. I. Baig, P. G. Ingole, W. K. Choi, J. D. Jeon, B. Jang, J. H. Moon and H. K. Lee, *Chem. Eng. J.*, 2017, **308**, 27–39.
51 M. I. Baig, P. G. Ingole, W. K. Choi, S. R. Park, E. C. Kang and H. K. Lee, *J. Membr. Sci.*, 2016, **514**, 622–635.
52 P. G. Ingole, R. R. Pawar, M. I. Baig, J. D. Jeon and H. K. Lee, *J. Mater. Chem. A*, 2017, **5**, 20947–20958.
53 M. I. Baig, P. G. Ingole, J.-d. Jeon, S. U. Hong, W. K. Choi and H. K. Lee, *Chem. Eng. J.*, 2019, **373**, 1190–1202.
54 Y. Shin, W. Liu, B. Schwenzer, S. Manandhar, D. Chase-Woods, M. H. Engelhard, R. Devanathan, L. S. Fifield, W. D. Bennett, B. Ginovska and D. W. Gotthold, *Carbon*, 2016, **106**, 164–170.
55 W. S. Hung, Y. L. Lai, P. H. Lee, Y. H. Chiao, A. Sengupta, M. Sivakumar, K. R. Lee and J. Y. Lai, *Sep. Purif. Technol.*, 2020, **239**, 116499–116506.

56 O. Tanskyi, Zeolite Membrane Water Vapor Separation for Building Air-Conditioning and Ventilation Systems, PhD, Texas A & M University, 2015.
57 T. D. Bui, Y. Wong, M. R. Islam and K. J. Chua, *J. Membr. Sci.*, 2017, **539**, 76–87.
58 D. Hopkinson, M. Zeh and D. Luebke, *J. Membr. Sci.*, 2014, **468**, 155–162.
59 Y. Y. Cao, Y. Chen, X. F. Sun, Z. M. Zhang and T. C. Mu, *Phys. Chem. Chem. Phys.*, 2012, **14**, 12252–12262.
60 F. J. Hernandez-Fernandez, A. P. de los Rios, F. Tomas-Alonso, J. M. Palacios and G. Villora, *J. Membr. Sci.*, 2009, **341**, 172–177.